Level set-based histology image segmentation with region-based comparison

Adel Hafiane, Filiz Bunyak, and Kannappan Palaniappan

Department of Computer Science,
University of Missouri-Columbia, Columbia, MO 65211 USA

***Abstract*— Automated histological grading of tissue biopsies for clinical cancer care is a challenging problem that requires sophisticated algorithms for image segmentation, tissue architecture characterization, global texture feature extraction, and high-dimensional clustering and classification algorithms. Currently there are no automatic image-based grading systems for establishing the pathology of cancer tissues. A primary step in computational histology is accurate image segmentation to detect significant regions such as nuclei, lumen and epithelial cytoplasm which together make up a gland structure. We describe a new approach for tissue segmentation using fuzzy spatial clustering and level set active contours. The proposed technique shows improvement in segmentation accuracy and outperform the classical clustering and level set methods, when compared to ground truth segmentation.**

I. Introduction

The availability of high resolution multispectral multimodal imaging of tissue biopsies provides a new opportunity to develop improved tissue segmentation algorithms for developing computer-aided diagnostic classification of histological images in a clinical setting. Automated quantitative grading of prostate cancer tissue patches that is beginning to compare favorably with visual analysis by experts for assigning a Gleason grade to histogological imagery was demonstrated using a combination of low level image texture features and high level graph-based tissue architecture features [1]. A multiresolution approach using global texture features including first- and second-order statistics combined with a Gabor filter set was able to achieve over 90% overall accuracy in distinguishing between cancerous and benign tissue, and nearly 77% in distinguishing between two complex grades of cancer (Gleason grade 3 and 4 adenocarcinoma). However, the architectural features of gland structures including spatial distribution of cell nuclei and the arrangement of glands were determined using manual segmentation in [1]. Recently, semi-automated image segmentation algorithms requiring prior probability estimates for the lumen structures and pixel-wise classification was developed to facilitate the extraction of spatial arrangement information [2]. In this paper, we develop a fully automatic robust image segmentation algorithm for histopathology imagery using fuzzy spatial clustering for class initialization, tissue class refinement using vector-based level sets or geodesic to accurately extract, nuclei, lumen and epithelial cytoplasm regions. The proposed techniques are compared with related approaches using qualitative and quantitative evaluation method.

The paper is organized as follows: Section II describes the Fuzzy C-means with spatial constraint algorithm, Section III presents the level sets multiphase scheme. Section IV describes the geodesic technique. The evaluation process is explained in section V results are given in Section VI, and the conclusions in Section VII.

II. Fuzzy C-means with spatial constraint

In this section we describe the method used to initialize the level set procedure. The FCM algorithm minimizes the objective function $J(U,V)$ which is defined by the sum of similarity measures. The objective function is given by

$$J(U,V) = \sum_{i=1}^{C}\sum_{j=1}^{N} u_{ij}^{m} \| \mathbf{x_j} - \mathbf{v_i} \|^2 \qquad (1)$$

where $X = \{\mathbf{x_1}, \mathbf{x_2}, ..., \mathbf{x_N}\}$ denote the set of data (pixel feature vector). $V = \{\mathbf{v_1}, \mathbf{v_2}, ..., \mathbf{v_C}\}$ represents the prototypes, known as the clusters centers. $U = [u_{ij}]$ is the partition matrix which satisfies the condition:

$$\sum_{i}^{C} u_{ij} = 1 \quad \forall j \qquad (2)$$

m is a fuzzifier which indicate the fuzziness of membership for each point. FCM algorithm is based on an iterative process by minimizing the distance between each point and the prototypes. The objective function Eq. 1 does not incorporate any spatial information. It is shown that the spatial information brings more robustness and efficiency to the fuzzy c-means algorithm [3], where a second term to include the spatial information is incorporated in the FCM objective function. This is expressed by the following equation:

$$\begin{aligned} J_M(U,V) &= \sum_{i=1}^{C}\sum_{j=1}^{N} u_{ij}^{m} \| \mathbf{x_j} - \mathbf{v_i} \|^2 \\ &+ \alpha \sum_{i=1}^{C}\sum_{j=1}^{N} u_{ij}^{m} \exp(-\sum_{k\in\Omega} u_{ik}^{m}) \end{aligned} \qquad (3)$$

where Ω is a set of neighbors. The parameter α is a weight that controls the influence of the second term (spatial information). The objective function (3) has two components. The first component is the same as FCM, the second is a penalty term. This component reaches a minimum when the membership value

of neighbors in a particular cluster is large. The optimization of (3) with respect to U have been solved by using Lagrange multiplier technique.

$$\begin{aligned} J_M(U,V) &= \sum_{i=1}^{C}\sum_{j=1}^{N} u_{ij}^m(\| \mathbf{x_j} - \mathbf{v_i} \|^2 + \alpha \exp(-\sum_{k\in\Omega} u_{ik}^m)) \\ &+ \sum_{j=1}^{N} \lambda_j (1 - \sum_{i=1}^{C} u_{ij}) \end{aligned} \quad (4)$$

the derivative of (4) with respect to u_{ij}

$$\frac{\partial J_M}{\partial u_{ij}} = m u_{ij}^{m-1}(\| x_j - v_i \|^2 + \alpha \exp(-\sum_{k\in\Omega} u_{ik}^m)) - \lambda_j \quad (5)$$

solving for u_{ij} we have

$$u_{ij} = \left(\frac{\lambda_j}{m(\| \mathbf{x_j} - \mathbf{v_i} \|^2 + \alpha \exp(-\sum_{k\in\Omega} u_{ik}^m))} \right)^{\frac{1}{m-1}} \quad (6)$$

solving for λ_j with respect to the constraint (2) we obtain

$$\sum_{i=1}^{C} \left(\frac{\lambda_j}{m(\| \mathbf{x_j} - \mathbf{v_i} \|^2 + \alpha \exp(-\sum_{k\in\Omega} u_{ik}^m))} \right)^{\frac{1}{m-1}} = 1 \quad (7)$$

As λ_j does not depend in the term of the sum this yield

$$\lambda_j^{\frac{-1}{m-1}} = \sum_{i=1}^{C} \left(m\| \mathbf{x_j} - \mathbf{v_i} \|^2 + \alpha \exp(-\sum_{k\in\Omega} u_{ik}^m) \right)^{\frac{-1}{m-1}} \quad (8)$$

The obtained membership update function is given by

$$u_{ij} = \frac{1}{\sum_{p=1}^{C} \left(\frac{\|\mathbf{x_j}-\mathbf{v_i}\|^2 + \alpha \exp(-\sum_{k\in\Omega} u_{ik}^m)}{\|\mathbf{x_j}-\mathbf{v_p}\|^2 + \alpha \exp(-\sum_{k\in\Omega} u_{pk}^m)} \right)^{\frac{1}{m-1}}} \quad (9)$$

The neighboring membership values (u_{pk}) influence u_{ij} to follow the neighborhood behavior. For instance if a given point has a high membership value to a particular cluster and its spatial neighbors have a small membership values to this cluster, the penalty term plays the role to force the point to belong to the same cluster as its neighbors. The weight α controls the importance of the regularization term. The prototype update equation is the same as standard FCM.

$$v_i = \frac{\sum_{j=1}^{N} u_{ij}^m x_j}{\sum_{j=1}^{N} u_{ij}^m} \quad (10)$$

The spatial constraint FCM (SCFCM) algorithm preforms the same steps as the original fuzzy c-means algorithm but, the membership function is computed according to the equation 9.

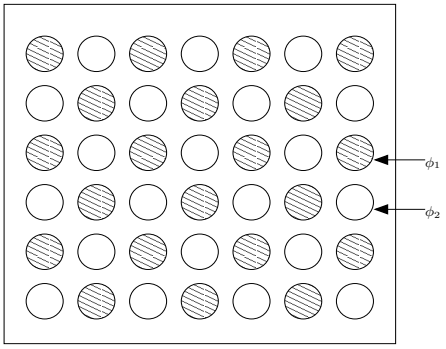

Fig. 1. A *multi-contour* level set initialization with two level set functions ϕ_1 and ϕ_2 (with no overlap), for segmenting a color image u_0.

III. Multiphase Vector-based Active Contours

In [4], Chan and Vese presented a multiphase extension of their two-phase level set image segmentation algorithm [5]. The multiphase approach enable efficient partitioning of the image into n classes using just $log(n)$ level sets without leaving any gaps or having overlaps between level sets. This ensures that each pixel is properly assigned to a unique class during the segmentation process. The Chan and Vese multiphase level set image segmentation approach involves minimization of a reduced or weak Mumford-Shah functional $F_n(\mathbf{c}, \Phi)$, otherwise referred to as a *minimal partition* Mumford-Shah functional [6]:

$$\begin{aligned} F_n(\mathbf{c},\Phi) &= \underbrace{\sum_{1\le i\le n=2^m} \lambda_i \int_\Omega (u_0 - c_i)^2 \chi_i \, d\mathbf{x}}_{\text{Energy Term}} \\ &+ \underbrace{\sum_{1\le i\le n=2^m} \mu_i \int_\Omega |\nabla \chi_i|}_{\text{Length Term}} \end{aligned} \quad (11)$$

where, n is the total number of classes associated with m level set functions, u_0 is the gray-level image being segmented, Φ is a vector of level set functions, $\mathbf{c}$ is a vector of mean gray-level values (i.e., $c_i = mean(u_0)$ of class or phase i), χ_i is the characteristic function for each class i represented by the associated Heaviside functions $H(\phi_i)$, and (λ_i, μ_i) are constants associated with each energy and length term of the functional $F_n(\mathbf{c}, \Phi)$. In order to simplify computation of the length term in the above reduced Mumford-Shah energy function, we replace the measure of the characteristic functions by the sum of the length of the zero-level sets of ϕ_i, $\sum_{1\le i\le m} \mu_i \int_\Omega |\nabla H(\phi_i)|$. Instead of an unweighted total length, this approximation weights some edges more than others, but is faster to compute and still leads to satisfactory segmentation results.

Chan and Vese also extended their two-phase level set image segmentation algorithm for scalar valued images to vector-valued images such as color or multispectral images [7] where the image is partitioned into piecewise constant vectors in the spirit of spatially-based vector quantization. In this paper we combine the multiphase approach with the feature vector approach to handle both multiple image classes and vector-

valued imagery such as segmenting color or multispectral images.

In the case of histopathology imaging derived from H&E stained cancer tissue biopsies four image classes have been shown to produce good feature sets for image classification-based cancer grading[1]. For the two level set case (i.e., $m = 2$) the image domain Ω is partitioned into *at most* four classes. Let $\mathbf{c} = \{\mathbf{c_{00}}, \mathbf{c_{01}}, \mathbf{c_{10}}, \mathbf{c_{11}}\}$ represent the set of average image feature vectors (ie three channel color) within each class or phase $\mathbf{c_{ij}}$, and $\Phi = (\phi_1, \phi_2)$ represent the two level set functions. The multiphase vector-based energy functional $F_n(\mathbf{c}, \Phi)$ is defined as,

$$\begin{aligned} F_n(\mathbf{c}, \Phi) =& \lambda_1 \int_\Omega \parallel \mathbf{u_0} - \mathbf{c_{00}} \parallel^2 \ (1 - H(\phi_1))(1 - H(\phi_2)) d\mathbf{x} \\ &+ \lambda_2 \int_\Omega \parallel \mathbf{u_0} - \mathbf{c_{01}} \parallel^2 \ (1 - H(\phi_1))H(\phi_2) \ d\mathbf{x} \\ &+ \lambda_3 \int_\Omega \parallel \mathbf{u_0} - \mathbf{c_{10}} \parallel^2 \ H(\phi_1)(1 - H(\phi_2)) \ d\mathbf{x} \\ &+ \lambda_4 \int_\Omega \parallel \mathbf{u_0} - \mathbf{c_{11}} \parallel^2 \ H(\phi_1)H(\phi_2) \ d\mathbf{x} \\ &+ \mu_1 \int_\Omega |\nabla H(\phi_1)| \ d\mathbf{x} + \mu_2 \int_\Omega |\nabla H(\phi_2)| \ d\mathbf{x} \quad (12) \end{aligned}$$

The Euler-Lagrange equations are obtained by minimizing Eq. 12 and embedding $\mathbf{c}$ and Φ in a dynamical system as [4]

$$\begin{aligned} \frac{d\phi_1}{dt} &= \delta(\phi_1)\Big\{\mu_1 \ \text{div}\big(\frac{\nabla\phi_1}{|\nabla\phi_1|}\big) \\ &\quad - \big\{(\lambda_1 \parallel \mathbf{u_0} - \mathbf{c_{11}} \parallel^2 - \lambda_3 \parallel \mathbf{u_0} - \mathbf{c_{01}} \parallel^2)H(\phi_2) \\ &\quad + (\lambda_2 \parallel \mathbf{u_0} - \mathbf{c_{10}} \parallel^2 - \lambda_4 \parallel \mathbf{u_0} - \mathbf{c_{00}} \parallel^2)(1 - H(\phi_2))\big\}\Big\}, \\ \frac{d\phi_2}{dt} &= \delta(\phi_2)\Big\{\mu_2 \ \text{div}\big(\frac{\nabla\phi_2}{|\nabla\phi_2|}\big) \\ &\quad - \big\{(\lambda_1 \parallel \mathbf{u_0} - \mathbf{c_{11}} \parallel^2 - \lambda_2 \parallel \mathbf{u_0} - \mathbf{c_{10}} \parallel^2)H(\phi_1) \\ &\quad + (\lambda_3 \parallel \mathbf{u_0} - \mathbf{c_{01}} \parallel^2 - \lambda_4 \parallel \mathbf{u_0} - \mathbf{c_{00}} \parallel^2)(1 - H(\phi_1))\big\}\Big\} \end{aligned} \quad (13)$$

where, $\mathbf{c_{ij}}$ is the mean vector of all pixel-based vectors associated with each class or phase.

$$\begin{aligned} \mathbf{c_{11}} &= \frac{\int_\Omega \mathbf{u_0} \, H(\phi_1) \, H(\phi_2) \, d\mathbf{x}}{\int_\Omega H(\phi_1) \, H(\phi_2) \, d\mathbf{x}} \\ \mathbf{c_{10}} &= \frac{\int_\Omega \mathbf{u_0} \, H(\phi_1) \, (1 - H(\phi_2)) \, d\mathbf{x}}{\int_\Omega H(\phi_1) \, (1 - H(\phi_2)) \, d\mathbf{x}} \\ \mathbf{c_{01}} &= \frac{\int_\Omega \mathbf{u_0} \, (1 - H(\phi_1)) \, H(\phi_2) \, d\mathbf{x}}{\int_\Omega (1 - H(\phi_1)) \, H(\phi_2) \, d\mathbf{x}} \\ \mathbf{c_{00}} &= \frac{\int_\Omega \mathbf{u_0} \, (1 - H(\phi_1)) \, (1 - H(\phi_2)) \, d\mathbf{x}}{\int_\Omega (1 - H(\phi_1)) \, (1 - H(\phi_2)) \, d\mathbf{x}} \end{aligned}$$

and $\delta(\phi_k) = H'(\phi_k)$ is the Dirac delta function. For numerical stability of the delta function, Chan and Vese propose using a regularized Heaviside function

$$H_{2,\epsilon}(x) = \frac{1}{2}\Big[1 + \frac{2}{\pi}\Big\{tan^{-1}\big(\frac{x}{\epsilon}\big)\Big\}\Big]$$

with

$$\delta_\epsilon(x) = \frac{1}{\pi} \, \frac{\epsilon}{\pi^2 + \epsilon^2}$$

The motivation for using a multiphase, rather than a two-phase, level set framework is to accurately detect adjacent regions that meet at a junction (i.e., the triple junction in [4]). However, as the number of regions grows exponentially with the number of level set functions, its best to use a small set of level set functions (typically two or three or equivalently, four or eight regions, respectively).

IV. Geodesic Level-sets Segmentation

In classical level set-based geodesic active contours [8], the level set function ϕ is evolved using the speed function,

$$\frac{\partial\phi}{\partial t} = g(\mathbf{u_0})(F_c + \mathcal{K}(\phi))|\nabla\phi| + \nabla\phi \cdot \nabla g(\mathbf{u_0}) \quad (14)$$

where F_c is a constant, $\mathcal{K}$ is the curvature term,

$$\mathcal{K} = div\left(\frac{\nabla\phi}{|\nabla\phi|}\right) = \frac{\phi_{xx}\phi_y^2 - 2\phi_x\phi_y\phi_{xy} + \phi_{yy}\phi_x^2}{(\phi_x^2 + \phi_y^2)^{\frac{3}{2}}} \quad (15)$$

and $g(\mathbf{u_0})$ is the edge stopping function. Edge stopping can be any decreasing function of the image gradient. For histopathology image segmentation, we use Beltrami color edge stopping function defined as

$$g(\mathbf{u_0}) = exp(-abs(\mathbf{det}(\mathcal{E}))) \quad (16)$$

where $\mathcal{E}$ is

$$\mathcal{E} = \begin{bmatrix} 1 + \sum\limits_{i=R,G,B} \Big(\frac{\partial \mathbf{u}_{0,i}}{\partial x}\Big)^2 & \sum\limits_{i=R,G,B} \frac{\partial \mathbf{u}_{0,i}}{\partial x}\frac{\partial \mathbf{u}_{0,i}}{\partial y} \\ \sum\limits_{i=R,G,B} \frac{\partial \mathbf{u}_{0,i}}{\partial x}\frac{\partial \mathbf{u}_{0,i}}{\partial y} & 1 + \sum\limits_{i=R,G,B} \Big(\frac{\partial \mathbf{u}_{0,i}}{\partial y}\Big)^2 \end{bmatrix} \quad (17)$$

The constant velocity F_c pushes the curve inwards or outwards depending on its sign. The regularization term $\mathcal{K}$ ensures boundary smoothness. The external image dependent force $g(\mathbf{u_0})$ is used to stop the curve evolution at object boundaries. The term $\nabla g \cdot \nabla\phi$ is used to increase the basin of attraction for evolving the curve to the boundaries of the objects.

The classical geodesic active contours is two phase and can segment an image into only two classes. In order to segment the three-class histopathology images we use two level sets, first level set segments the lumen regions from the rest of the image, second level set segments nuclei regions from the rest of the image. Both level sets are initialized outside of their region of interest (lumen and nuclei regions respectively) and to move inwards. SCFCM mask (Section II) is used for initialization, two binary masks one for lumen one for nuclei classes are produced from the multi-class SCFCM mask (1-for lumen 0-for everything else and 1-for nuclei and zero for everything else respectively). Both masks are dilated with a large enough structuring element to ensure that they fully contain the regions of interests. The geodesic active contours are initialized from the dilated masks.

V. Evaluation

To evaluate the segmentation accuracy we use supervised criterion [9]. The criterion is based on region overlapping where each region from the segmented image is overlapped with each region of the ground truth image. The high percentage of the overlapping indicate how much the two images are close comparing each other. However the under-segmentation can provide large overlapping areas which introduce miss estimation in segmentation quality. The used criterion take into account this aspect and penalize either the under-segmentation or over-segmentation. The evaluation measure incorporate the following points:

- *Localization: the detected regions should be spatially coherent (eg. position, shape, size...) with those present in the reference,*
- *Over-segmentation: this situation is considered as disturbing and has to be penalized in the quality index,*
- *Under-segmentation: this situation is considered as a segmentation error and has also to be penalized.*

Let R_i^{Ref} and R_j^{Seg} be two classes belonging respectively to the reference I^{Ref} and to the segmentation result I^{Seg} ($i = 1..NR_{Ref}$, $j = 1..NR_{Seg}$ where NR_{Ref} is the number of regions of the reference and NR_{Seg} the number of regions of the segmentation result. The matching index M_I is over all regions is given by:

$$M_I = \sum_{j, max_i Card(R_i^{Ref} \cap R_j^{Seg})} \frac{Card(R_i^{Ref} \cap R_j^{Seg})}{Card(R_i^{Ref} \cup R_j^{Seg})} \rho_j \quad (18)$$

where $Card(X)$ is the number of pixels of X. The weighting factor ρ_j expresses the importance of the region j in the image and permits to give to small regions less influence in the quality measure.

$$\rho_j = \frac{Card(R_j^{Seg})}{Card(I^{Seg})} \quad (19)$$

The equation (18) express a morphological relation between two regions/classes. Each class of a segmentation result is compared with the corresponding one in the reference by taking into account the maximum overlapping surface. For instance, if there are two regions in I^{Seg} that intersect with a region of I^{Ref}, the measure considers the maximum of intersection. However, the no perfect matching is penalized by the normalization term $Card(R_i^{Ref} \cup R_j^{Seg})$. In the case of the perfect matching the index M_I is equal to 1.

The over- and under-segmentation errors are described by

$$\eta = \begin{cases} NR_{Ref}/NR_{Seg} & if \quad NR_{Seg} \geq NR_{Ref} \\ log(1 + NR_{Seg}/NR_{Ref}) & otherwise \end{cases} \quad (20)$$

The final evaluation criterion $\mathcal{H}$ is then given by the following equation:

$$\mathcal{H} = \frac{M_I + m \times \eta}{1 + m} \quad (21)$$

where m is a weighting coefficient which controls the importance of the over-/under-segmentation errors in the judgment. As shown in [9] $m = 0.2$ realize a good trade off between between different evaluation parameters. For the all experiment m is set to 0.2.

VI. Results and discussion

The experiments have been performed over histopathology images[1]. We applied clustering based methods, Level set based active contours segmentation methods and combination of both. The tested clustering methods are: K-means, Fuzzy C-means, and SCFCM (see section II). We have used two categories of level sets methods multi-phase described in section III and geodesic described in section IV. Figure 2 shows the segmentation results of the different techniques. Figure 2(a) represents the original images Gleason Grade 3 tissue composed of nuclei, lumen, and epithelial cytoplasm. Next, figure 2(b) the manual segmentation with 3 classes: red (nuclei), green (lumen) and yellow (cytoplasm).

The result of k-means and FCM algorithms are shown respectively in figure 2(c) and figure 2(d). The two algorithms provide similar results. Both methods produce more lumen regions compare to the ground truth. This is partly because some small dominantly white regions within the cytoplasm are not finely classified in the coarse manual segmentation and partly because both K-means and Fuzzy C-means do not incorporate any spatial information and tend to fragment regions. The SCFCM overcome the latter deficiency using spatial correlation to reduce this effect as shown in figure 2(e), the segmented regions look more spatially coherent but the segmentation is still poor comparing to the ground truth.

Both of the level set-based segmentation approaches geodesic figure 2(f) and vector multiphase (figures 2(g), 2(h)) improve the segmentation quality and provide more accurate regions. But for histopathology image segmentation, vector multiphase level is more reliable and robust compared to geodesic active contours. Geodesic active contours is more sensitive to initialization (should start either completely inside or outside of the regions of interest). It suffers from contour leaking on weak edges (ie. some nuclei edges), and early stopping on background edges (ie. cytoplasm texture). Due to these problems some significant nuclei regions disappear (figure 2(f)).

The multiphase vector-based level set (MVLS) is used with two different initialization concepts: random circles (figure 1) and SCFCM segmented regions. As expected MVLS combined with SCFCM (figure 2(h)) produces better results than MVLS (figure 2(g)) with random initialization specially in the lumen regions. MVLS-SCFCM segmentation results appear more accurate than the other algorithms comparing to the original image and the ground truth. Statistics of algorithms comparison is explained in the next paragraph.

Table I compares performance of different segmentation methods for each class in terms of area percentage Eq. 22,

[1]Histopathology imagery provided by Michael Feldman (Dept. of Surgical Pathology, Univ. of Pennsylvania) and ground truth from Anant Madabhushi (Rutgers).

Method	Area %			Overlap %			Normalized overlap %		
	Class 1	Class 2	Class 3	Class 1	Class 2	Class 3	Class 1	Class 2	Class 3
Ground truth	28.6	11.1	60.3	-	-	-	-	-	-
K-means	28.2	37.5	34.0	22.2	10.3	28.2	65.0	27.4	42.3
FCM	28.1	37.8	34.1	22.4	10.4	28.1	65.3	27.0	42.5
SCFCM	26.8	32.1	41.2	21.6	10.3	34.1	64.1	31.2	50.7
Geodesic-SCFCM	27.3	16.7	56.0	21.2	9.1	47.2	61.2	48.8	68.3
MVLS-random	28.9	23.6	47.6	22.3	9.9	40.5	63.3	40.2	60.1
MVLS-SCFCM	27.7	20.4	51.9	22.2	9.6	44.3	65.3	43.9	65.3

TABLE I

COMPARISON STATISTIC MEASURES

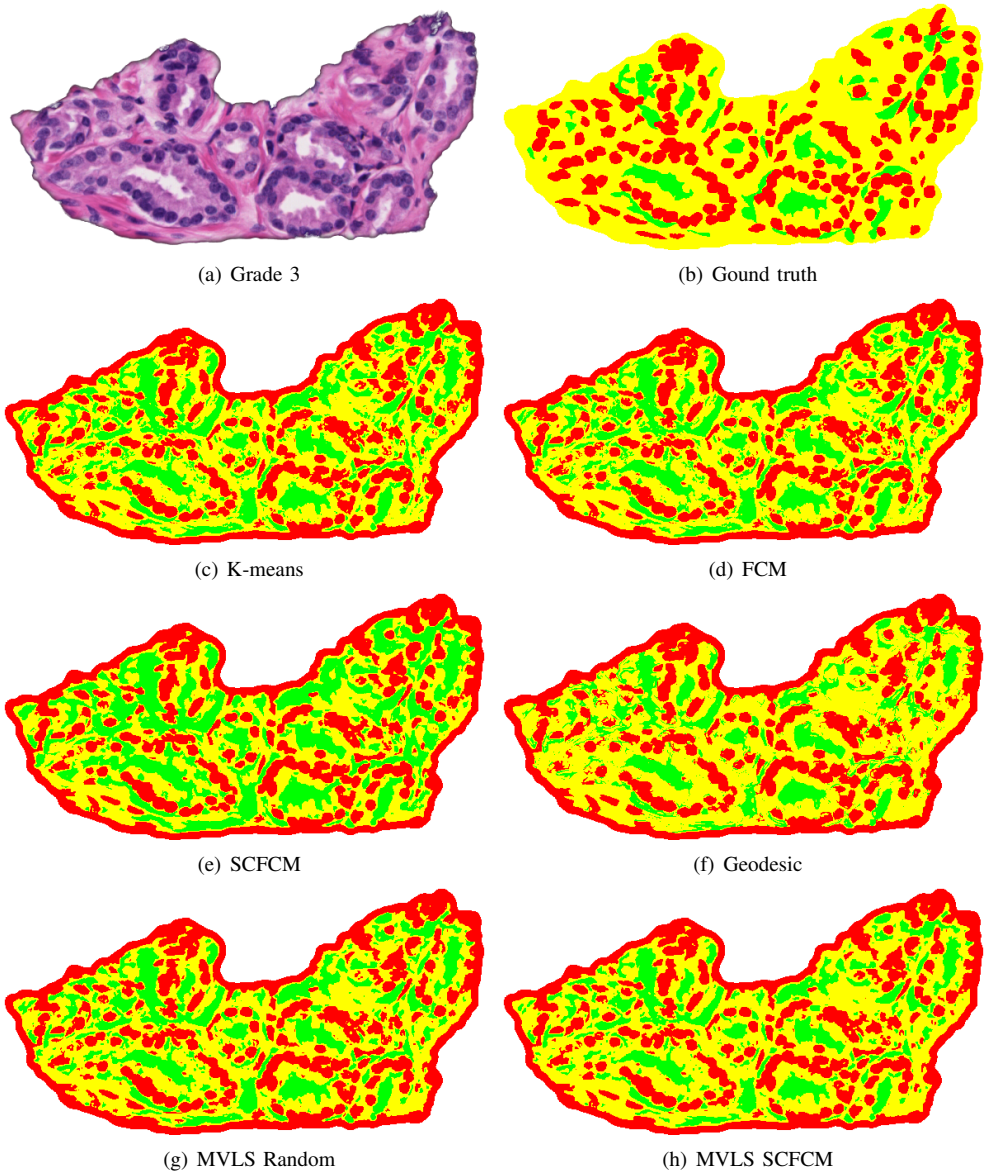

(a) Grade 3 (b) Gound truth

(c) K-means (d) FCM

(e) SCFCM (f) Geodesic

(g) MVLS Random (h) MVLS SCFCM

Fig. 2. Automatic segmentation of Gleason grade 3 histopathology image with nuclei shown in red, lumen in green, epithelial cytoplasm in yellow.

overlap percentage Eq. 23, and normalized overlap percentage Eq. 24. These additional measures comes to enforce the evaluation criteria described in Section V. In table I Class 1, Class 2, and Class 3 represent nuclei, lumen and cytoplasm classes respectively.

$$\texttt{Area} = \frac{card(R_i)}{\texttt{Total number of points}} \times 100 \qquad (22)$$

$$\texttt{Overlap} = \frac{Card(R_i^{Ref} \cap R_i^{Seg})}{\texttt{Total number of points}} \times 100 \qquad (23)$$

$$\texttt{Normalized overlap} = \frac{Card(R_i^{Ref} \cap R_i^{Seg})}{Card(R_i^{Ref} \cup R_i^{Seg})} \times 100 \qquad (24)$$

Distribution of the different classes in the reference image is: nuclei 29%, lumen 11%, and cytoplasm 60%. For the nuclei class all tested algorithms provide areas similar to the area in the reference image. The major difference reside in lumen and cytoplasm classes due to the additional small lumen regions detected. Geodesic-SCFCM produces the best results for the area measure, followed by MVLS-SCFCM. The overlap measures between ground truth class and the corresponding one in the automatic segmentation are given in third major column of the table I. There are high overlap percentages for nuclei, but much less for lumen and cytoplasm. Level set methods provides better spatial precision particularly for lumen class. They tend to shrink lumen and nuclei regions, this reduces the overlap area with the reference image. Although the low percentage of overlapping in lumen area, level set methods provides better results in terms of accuracy and localization. This is shown in the next fourth major column of table I. For the nuclei class all the methods presents good performances 64% in average. The lumen class produces low percentage 27% for K-means and FCM, 31% for SCFCM, Geodesic-SCFCM with 48%, MVLS-Random 40% and MVLS-SCFCM provides 43%. For cytoplasm class the level set algorithms give better results an average of 64%.

As more reliable measures, we compute the criteria $\mathcal{H}$ Eq. 21 and M_I Eq 18 (see section V). These criteria are not symmetric, so the measure is applied in two different ways, automatic segmented image (Seg) versus groud truth (GT) and vice versa. Table II shows the segmentation quality compared to the reference image over all classes. Geodesic-SCFCM gives higher values for M_I measure producing 78% closer to the reference image. But when the over-under segmentation penalty is introduced in $\mathcal{H}$ criterion, MVLS-SCFCM outperforms all the tested methods.

VII. Conclusion

In this paper we described a robust algorithm for fully automatic tissue segmentation of glandular structures in histopathology imagery. An accurate unsupervised initialization is provided using the spatial constraint fuzzy c-means developed previously by our group. The initial image clusters which may not be spatially contiguous with biological regions of interest are refined using an extended active contour algorithms to handle complex biological structures in color imagery. We evaluate the segmentation accuracy according to the manual segmentation (ground truth). The proposed method outperforms the classical methods for all classes of regions, nuclei, lumen and cytoplasm. The quality of segmentation is important since it will be used for tissue classification in further future work.

References

[1] S. Doyle, M. Hwang, K. Shah, A. Madabhushi, M. Feldman, and J. Tomaszeweski, "Automated grading of prostate cancer using architectural and textural image features," in *IEEE Int. Symp. Biomedical Imaging: From Nano to Macro*, April 2007, pp. 1284–1287.

[2] S. Naik, S. Doyle, M. Feldman, J. Tomaszewski, and A. Madabhushi, "Gland segmentation and computerized Gleason grading of prostate histology by integrating low-, high-level and domain specific information," in *Proc. 2nd MICCAI Workshop Microscopic Image Analysis with Appl. in Biology (MIAAB)*, Piscataway, NJ, USA, 2007.

[3] A. Hafiane, B. Zavidovique, and S. Chaudhuri, "A modified FCM with optimal Peano scans for image segmentation," in *IEEE ICIP*, Genova, Italy, 2005.

[4] L. Vese and T. Chan, "A multiphase level set framework for image segmentation using the Mumford and Shah model," *Int. J. Computer Vision*, vol. 50, no. 3, pp. 271–293, 2002.

[5] T. Chan and L. Vese, "Active contours without edges," *IEEE Trans. Image Proc.*, vol. 10, no. 2, pp. 266–277, Feb. 2001.

[6] D. Mumford and J. Shah, "Optimal approximations by piecewise smooth functions and associated variational problems," *Comm. Pure Appl. Math.*, vol. 42, pp. 577–685, 1989.

[7] T. Chan, B. Sandberg, and L. Vese, "Active contours without edges for vector-valued images," *J. of Visual Communication and Image Representation*, vol. 11, pp. 130–141, 2000.

[8] V.Caselles, R.Kimmel, and G.Sapiro, "Geodesic active contours," *Int. J. Computer Vision*, vol. 22, no. 1, pp. 61–79, 1997.

[9] A. Hafiane, S. Chabrier, C. Rosenberger, and H. Laurent, "A new supervised evaluation criterion for region based segmentation methods.," in *ACIVS*. 2007, vol. 4678 of *Lecture Notes in Computer Science*, pp. 439–448, Springer.

Algorithm	M_I %	$\mathcal{H}$ %	M_I %	$\mathcal{H}$ %
	Seg → GT	Seg → GT	GT → Seg	GT → Seg
K-means	69.1	60.0	68.5	60.6
FCM	69.0	60.1	68.8	60.06
SCFCM	72.0	64.6	69.2	62.9
Geodesic-SCFCM	**78.9**	68.2	**78.35**	67.9
MVLS-random	75.8	67.8	71.4	64.9
MVLS-SCFCM	78.2	**70.8**	73.6	**68.1**

TABLE II
SEGMENTATION EVALUATION USING M_i AND $\mathcal{H}$ CRITERIA